Title of the Manuscript:

Concentration polarization around polyelectrolyte-coated electrodes. Model and observations

J.A. Lirio-Piñar[1], S. Orozco-Barrera[1], A.V. Delgado[1,2,3], S. Ahualli[1,2*]

[1]*Departamento de Física Aplicada, Facultad de Ciencias, Universidad de Granada, 18071 Granada, Spain*

[2]*MNat Unit of Excellence, University of Granada, Spain*

[3]*Instituto de Investigación Biosanitaria, IBS Granada*

*Corresponding author:

Silvia Ahualli

Departamento de Física Aplicada, Facultad de Ciencias

Universidad de Granada, 18071 Granada, Spain

E-mail: sahualli@ugr.es

Abstract

An investigation on the phenomenon of concentration polarization (CP) in conducting porous particles is presented in this work, considering both bare and polyelectrolyte-coated particles. The conducting nature of the porous structure brings about the induction of a surface (and hence volume) charge distribution by the applied external field. The polymer charge (with its counterions from solution) is superimposed on this field-induced component. From the solution of Poisson's equation, the concentration and potential profiles are evaluated, and from them, the concentration polarization can be calculated. The results are presented as concentration perturbation as a function of time after application of the field, both for bare and coated particles. Experiments are also performed aimed at measuring the CP using a solution of fluorescent dye (rhodamine B). From the increase or decrease of fluorescence, the concentration perturbations are observed around the particle. Importantly, depletion of concentration is observed on both sides of the particle when this is bare. In contrast, if the particles are coated, the classical pattern of a pole of increased concentration and an opposite one of decreased concentration is found. Dielectric dispersion experiments in suspensions of bare and brush-coated particles confirm this fact.

Key words: activated carbon; CDI; concentration polarization; conducting porous particles; polyelectrolyte coating

1. Introduction

Electrochemical methods for energy production and storage [1-6], and solution deionization [7-11] are gaining increased interest because of their ease of application, considerable efficiency, and accessibility. In the particular case of deionization of solutions down to admitted salinity levels for drinking has received a lot of attention, as, due to the climate change, there is a rising lack of safe drinking water, and hence capacitive deionization (CDI) is a current issue where there have been many advances in the last two decades. To mention just a few examples, new materials for the electrodes are being tested [10], in addition to more complex geometries for desalination cells [11, 12], or even the use of a number of rotating electrodes [14].

In all cases, the basic phenomena deal with the large surface/volume ratio of the electrode, and the building up of electrical double layers (EDLs) compensating for the electronic charge on the electrodes. It is in the formation of the EDLs that the ability of the system lies for producing (through salinity exchange of the solution in contact with the electrodes) or storing (through mobile charge accumulation) energy, or for desalinating solutions (ions in the EDLs are removed from the solution) [12].

Most experimental works in the field have focused on the investigation of materials suitable for electrodes, regarding their overall porosity, stability, electrical conductivity, etc. [13-16]. However, significant contributions can be cited in relation to functionalization of the electrodes prior to implementing them in the conductivity cell. Following promising results obtained with ion-exchange membranes located on top of the electrodes (membrane CDI or MCDI), the use of polyelectrolytes directly deposited from solution onto them (soft-electrodes CDI) has also been demonstrated to be an efficient alternative [17-22]. There is still a step forward, focusing on the fundamental aspects of CDI (and not so much on the technical issues, important as they are): this is taking advantage of the phenomenon of concentration polarization (CP) for capacitive deionization.

Recall that CP is the accumulation of clouds of increased (decreased) concentration of electrolyte on each side of the particle due to the application of an electric field, and it is the result of the fact that the transport number of coions and counterions differ significantly in the vicinity of a highly charged interface [23]. This phenomenon is especially relevant in devices that integrate nanoporous materials and microscale systems,

such as hybrid nano/microfluidic architectures used for separation, or detection [24, 25] focused on a broad range of applications. The advantage of CP in desalination of solutions and shock electrodialysis has been recently investigated by Montes et al. [26], and the contributions of Bazant and collaborators [27-29]. However, in these structures CP is as relevant as complex because of the mechanisms involved in the mass and charge transport, hence a deep understanding of it and a theoretical model can be the key to the improvement in performance of the applications mentioned. From the experimental point of view, direct observations using fluorescent ions in solution obtained for a millimeter-sized cylinder can be mentioned [30], where the authors state that CP can lead to the removal of a significant number of ions building the polarization clouds.

Although the phenomenon has been explored in CDI [29, 31, 32], no such attempts have been reported if polyelectrolyte-coated electrodes are used. It is hence of interest to check if polyelectrolyte functionalization of porous carbon can affect the salt concentration clouds associated to CP. So, in this paper we will first elaborate a model of CP in the case of soft porous conductive particles of activated carbons, and then describe our experiments on the polarization of both bare and coated particles, including polyelectrolyte layers adsorbed and grafted on the carbons. The analysis will be based on a direct visualization of the phenomenon using fluorescence microscopy, which make it possible to learn about the electrical properties of the system. Furthermore, the CP phenomenon is indirectly detected in determinations of dynamic electrophoretic mobility (that is, electrophoretic mobility of the particles in ac fields) or in dielectric dispersion of suspensions [33, 34]. Such studies have never been attempted in the case of porous conductive carbon, either coated or bare, and this is another aim of the present contribution.

2. Model

2.1. Effect of an applied electric field on a functionalized porous conductive particle

The aim of this simple model is to be able to understand the far from trivial mechanisms that take place in this phenomenology. Other theoretical developments explain in a more rigorous way the problem [30] but this model, used for insulating particles, has the advantage of allowing us to delve into the mechanisms that occur at the porous conductive solid/liquid interface in the presence of an applied electric field.

Although when an electric field is applied to a conducting particle all mechanisms occur at once, in this model we will consider that they take place in two stages. The first response we will consider is the formation of an EDL caused by the charge induced by the electric field. And the second step is the appearance of concentration gradients produced by the spatial difference in the ionic transport numbers.

The model developed will be based on a simple description of the particles constituting the porous electrode. As shown in Fig. 1, three well distinguishable regions are identified. We assume that we are working with spherical porous conducting particles, containing two populations of pores: mesopores, with several micrometer diameter, and micropores, in the range of at most a few nm. This somewhat artificial division will demonstrate to be important in the characterization of our particles because the behavior of ions and polymer will be different in each kind of pores.

The inner region is a spherical and impenetrable core of radius *a*. Here, in order to simplify the calculations, we assume that there is not any charge: the ions and the polymer coating are not able to reach this zone.

In the layer of thickness *L*, three effects overlap:

- Since the particle is conducting, charge can be induced by the application of an electric field **E**.
- Ions can penetrate inside this zone both in micro- and mesopores.
- In the case of a polymer-based coating, this is assumed to be charged by ionization of the polymer chains. This charge will be counterbalanced by ions from the solution.

This approach considers that the induced charge provoked by the electric field is distributed in outer region ($a \le r \le a + L$). As the micropores sizes are very narrow (typically a few nanometers), many authors consider that a Donnan-type potential distribution is established.

Finally, outside of the particle we have a certain distribution of ions forming a diffuse double layer.

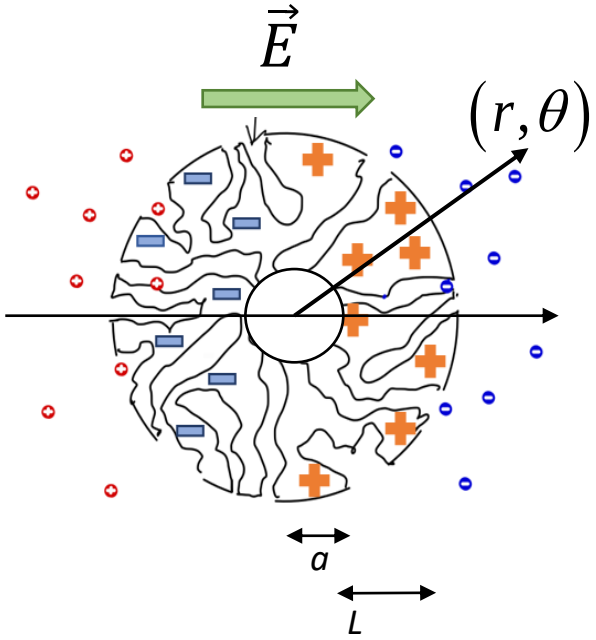

Figure 1. Simplified view of the structure of the porous particle. *a* is the radius of the rigid core, and *L* is the thickness of the charged layer. The + and – signs in the layer indicate the charges in it; the red and blue circles are cations and anions in the solution. The electric field **E** and the polar coordinates are indicated.

Since we are seeking to find the potential and ion concentration profiles, we begin by writing Poisson equation for the different regions:

$$\nabla^2\Psi(\mathbf{r}) = \begin{cases} 0 & \text{for} \quad r \le a \\ -\dfrac{1}{\varepsilon_m\varepsilon_0}\left(\sum_i ez_i n_i(\mathbf{r}) - \rho_{ind}(\mathbf{r}) - \rho_{pol}\right) & \text{for} \quad a \le r \le a+L \\ -\dfrac{1}{\varepsilon_m\varepsilon_0}\sum_i ez_i n_i(\mathbf{r}) & \text{for} \quad a+L \le r \end{cases} \qquad (1)$$

In these equations, $\Psi(\mathbf{r})$ is the electric potential at position **r**, $\varepsilon_m\varepsilon_0$ is the permittivity of the medium, $z_i e$ is the charge of the *i*-th ionic species ($i = 1,\ldots,N$), and $n_i(\mathbf{r})$ its number concentration at position **r**. In addition, ρ_{ind} is the volume charge density induced by the electric field, and ρ_{pol} is that provided by the polymer coating.

The induced charge density can be calculated after decomposing the field into radial and tangential components, and considering that the field is the superposition of the external and dipolar components:

$$\begin{aligned} E_r &= E\left(1+\frac{2a^3}{r^3}\right)\cos\theta \\ E_\theta &= -E\left(1-\frac{a^3}{r^3}\right)\sin\theta \end{aligned} \tag{2}$$

The surface charge density will then be given by:

$$\sigma_{ind} = \varepsilon_m\varepsilon_0\, E_r\big|_{r=a} = 3\varepsilon_m\varepsilon_0 E\cos\theta \tag{3}$$

Since this surface charge is spread on the surface of the pores, it will give rise to an induced volume charge density (considering a modified-Donnan model for the micropores) with the same angular dependence,

$$\rho_{ind} = \rho_0\cos\theta \tag{4}$$

where ρ_0 is an adjustable parameter and it will be a function of the applied electric field modulus, due to the surface charge dependence (c.f. eq. (3)).

Using separation of variables, the electric potential can be written as:

$$\Psi(\mathbf{r}) = \psi(r)\mathbf{E}\cdot\hat{\mathbf{r}} = \psi(r)E\cos\theta \tag{5}$$

and the Laplacian in eq. (1) can be expressed, after substitution of eq. (5):

$$\nabla^2\Psi(\mathbf{r}) = \left(\frac{d^2\psi}{dr^2}+\frac{2}{r}\frac{d\psi}{dr}-\frac{2}{r^2}\psi\right)E\cos\theta \tag{6}$$

The rhs side of eq. (1) outside the polymer layer will read:

$$-\frac{1}{\varepsilon_0\varepsilon_m}\sum_i ez_i n_i(\mathbf{r}) = -\frac{1}{\varepsilon_0\varepsilon_m}\sum_i ez_i n_i(\infty)\exp\left(-\frac{ez_i\psi(r)E\cos\theta}{k_BT}\right), \quad i=1,...,N \tag{7}$$

where $n_i(\infty)$ is the concentration of ions in the bulk solution, and k_BT is the thermal energy. Finally, the Poisson-Boltzmann equation can be written:

$$\left(\frac{d^2\tilde{\psi}}{dr^2}+\frac{2}{r}\frac{d\tilde{\psi}}{dr}-\frac{2}{r^2}\tilde{\psi}\right) = -\frac{1}{\varepsilon_0\varepsilon_m}\sum_i ez_i n_i(\infty)\exp\left(-\frac{ez_i\tilde{\psi}}{k_BT}\right), \quad i=1,...,N \tag{8}$$

where $\tilde{\psi}(r;\theta) = \psi(r) E \cos\theta$ depends parametrically on θ. This equation can be numerically solved for any value of θ using a Matlab© routine (BVP4C). The boundary conditions for the potential $\tilde{\psi}(r)$ are:

$$\left.\frac{d\tilde{\psi}}{dr}\right|_{r=a} = 0 \qquad \left.\frac{d\tilde{\psi}}{dr}\right|_{r\to\infty} = 0 \tag{9}$$

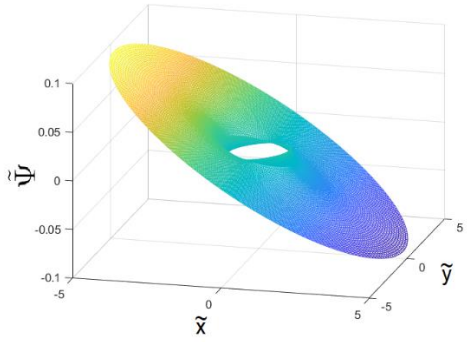

Figure 2: Non-dimensional total (uniform term + dipolar term) electric potential profile.

The superposition of the electric potential solving the equations (8) and boundary conditions (9) and the uniform term due to the applied electric field give an almost constant potential in the region of porous, and a decay as a typical from EDL to the value reaching far from the particle but with an angular dependence (Fig.2).

2.2 Analysis of concentration polarization

Once the potential profile is solved as described, it is possible to find the concentration variations associated to polarization. This can be done in analytical form by making use of an analogy with a well-known solved problem, namely, the potential around a charged, surface-conducting sphere. We start from the conservation of the number of ions, by making their flux divergence equal to zero:

$$\nabla \cdot \mathbf{j}^i = 0, \quad i = 1, ..., N \tag{10}$$

The flux of the *i*-th ions is composed of three terms: an electric one corresponding to the interaction with the electric field, a diffusive one associated to concentration gradients,

and a convective term associated to the motion of the liquid around the particle. According to Derjaguin-Dukhin and Dukhin-Shilov theory [35, 36], all these terms can be obtained from gradients of scalar quantities. This is easy to see by considering the electrochemical potential, (from now on, we will focus on the realistic case of solutions containing only two ionic species, one positive and one negative with valencies $+z$ and $-z$, respectively):

$$\mathbf{j}^{\pm} = -\frac{D^{\pm}}{k_B T} n^{\pm} \nabla(\mu_e{}^{\pm} + \mu_d{}^{\pm} + \mu_c{}^{\pm}) = -\frac{D^{\pm}}{k_B T} n^{\pm} \nabla \mu^{\pm} \tag{11}$$

being $D^{+}(D^{-})$ the diffusion coefficient of cations (anions).

By combining eqs. (10),(11), the differential equation governing our problem is:

$$\nabla^2 \mu^{\pm} = 0 \tag{12}$$

Regarding boundary conditions, the first one comes from the fact that the only term remaining when we are far enough from the particle surface is the electric contribution:

$$\nabla^2 \mu^{\pm}\Big|_{\infty} = \mp ezE \tag{13}$$

The second boundary condition regards the EDL formed at the particle/solution interface. If we suppose that concentration is enough to have a very thin EDL, then the only source of ions in the EDL is their flow perpendicular to the surface:

$$\mathbf{j}^{\pm} \cdot \hat{\mathbf{r}}\Big|_{r=a+L+x_D} = \nabla \cdot \mathbf{j}_S^{\pm}\Big|_{r=a+L+x_D} \tag{14}$$

Here, x_D is the Debye length (or EDL thickness), and $\mathbf{j}_S^{\pm}$ is the surface flux of each kind of ion. Thinking of the formal parallelism between the electrical and chemical potential equations, we can establish the similarities described in Table 1.

Starting from the well-known solution to the problem for electric current, the solution for electrochemical potential is identical, but modifying coefficients according to changes in boundary conditions. Thus, the following expression can be proposed:

$$\mu^{\pm}(r,\theta) = \mp ezEr\cos\theta \pm ezEL^3 \frac{R^{\pm} - 1}{R^{\pm} + 2} \frac{\cos\theta}{r^2} \tag{15}$$

Table 1. Formal similarities between the equations and boundary conditions for the electrochemical and electrical potentials.

Electrochemical potential, μ	Electrical potential, Ψ
$\nabla^2\mu^{\pm}=0$	$\nabla^2\Psi=0$
$\mathbf{j}^{\pm}=-\frac{D^{\pm}}{k_BT}n^{\pm}\nabla\mu^{\pm}$	$\mathbf{i}=-K\nabla\Psi$
$\nabla\cdot\mathbf{j}^{\pm}=0$	$\nabla\cdot\mathbf{i}=0$
$\nabla^2\mu^{\pm}\big\vert_{\infty}=\mp ezE$	$\nabla^2\Psi\big\vert_{\infty}=-E$
$\mathbf{j}^{\pm}\cdot\hat{r}\big\vert_{r=a+L+x_D}=\nabla\cdot\mathbf{j}^{\pm}{}_{\text{sup}}\big\vert_{r=a+L+x_D}$	$\mathbf{i}\cdot\hat{r}\big\vert_{r=a+L+x_D}=\nabla\cdot\mathbf{i}_{\text{sup}}\big\vert_{r=a+L+x_D}$

where $R^{\pm}$ is twice the Dukhin number for each type of ion [36]:

$$R^{\pm}(\theta)=2Du^{\pm}(\theta)=\frac{4x_D}{L}\left[\exp\left(\mp\frac{z\tilde{\psi}(a;\theta)}{2k_BT}\right)-1\right]\left(1-3m^{\pm}\right)\pm\frac{6x_Dm^{\pm}\tilde{\psi}(a;\theta)}{Lk_BT} \tag{16}$$

with

$$m^{\pm}=\frac{2\varepsilon_0\varepsilon}{3\eta D^{\pm}}\left(\frac{k_BT}{ze}\right)^2 \tag{17}$$

characterizing the relative contribution of convection to surface conductance, η being the viscosity of the fluid.

Once we have an expression for the electrochemical potential, we can use its definition (11) to obtain an equation for concentration variations:

$$\frac{\Delta n(\theta)}{n^{\pm}(\infty)}=\frac{ezE\cos\theta}{2k_BT}\frac{L^3}{r^2}\left[\frac{R^+-1}{R^++2}-\frac{R^--1}{R^-+2}+\frac{3(R^+-R^-)\left(\frac{U^+}{R^++2}+\frac{U^-}{R^-+2}\right)}{(R^++2)(R^-+2-U^-)+(R^-+2)(R^++2-U^+)}\right] \tag{18}$$

where, according to the model proposed by Uppapalli and Zhao [37],

$$U^{\pm} = \frac{48 x_D m^{\pm}}{L} \ln\left[\cosh\left(\frac{z\tilde{\psi}(a;\theta)}{4k_B T}\right)\right] \tag{19}$$

To conclude, equation (18) provides us with a tool to calculate the changes in ion concentration in the EDL for a conducting particle immersed in a salt solution under an electric field.

3. Experimental

3.1 Materials

The activated carbon investigated was YP50 (Fig. 3) from Kuraray Co. Ltd. (Japan). According to the manufacturers, the surface area of this carbon is 1692 m^2/g, with most of the porosity ranging between 1 and 2 nm. The specific capacitance of the sample is 18 F/g. All other chemicals used were purchased from Sigma Aldrich (Merck Life Science, Germany). The water employed in the solution preparation was deionized and filtered in a Milli-Q Academic (Millipore, France) system.

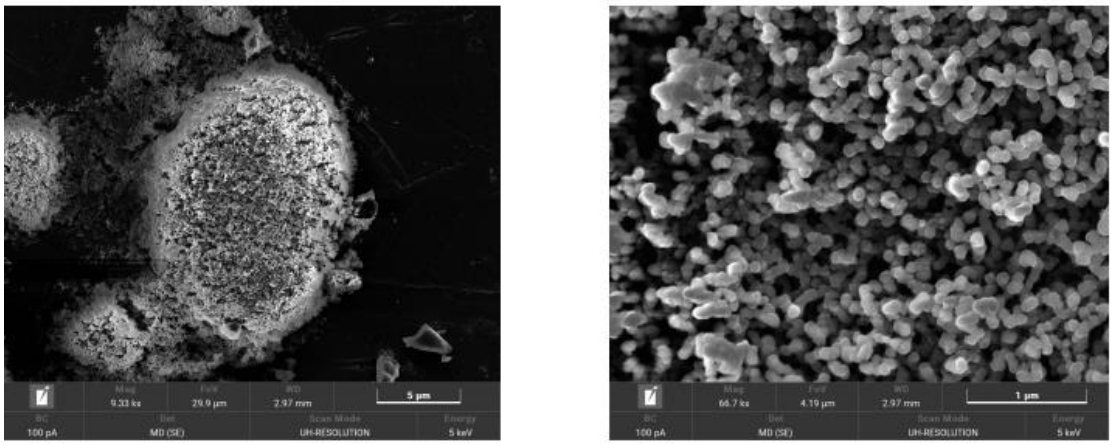

Figure 3. SEM micrographs of YP50 carbon particles.

3.2 Methods

Polyelectrolyte coating of the carbons

For the polyelectrolyte coating, 500 mg of carbon powder was immersed overnight in 250 mL of a 200 mM (on a monomer basis) PDADMAC (or PSS) aqueous solution under constant magnetic stirring, thus producing a positive (or negative) layer.

The product was then centrifuged, and the supernatant was removed. The sample was redispersed in H_2O and the washing procedure was repeated twice. Then, the coated carbon was left to dry at 50 °C overnight.

Preparation of brush-grafted carbons

The grafting of the carbon required a two-step procedure: activation with 4-vinylaniline radicals and polymerization. For the activation, 250 mL of a carbon aqueous suspension was prepared (10 g of carbon). The suspension was magnetically stirred throughout the whole process. Once initially mixed, 0.78 mL of a 37% wt. HCl aqueous solution were added to the suspension. After 40 minutes, 0.375 g of 4-vinylaniline was added to the mixture, which was heated to 43 °C during 10 more minutes. Once the temperature was reached, a solution of 0.15 g of $NaNO_3$ in 10 mL of H_2O was slowly added along 15 minutes. The product was kept under magnetic stirring and at 43 °C for 16 hours. Then, it was centrifuged for 20 minutes at 20 000 rpm, the supernatant was removed, and acetone was added. The product was redispersed and again centrifuged, then vacuum-dried at 35 °C overnight. The 4-vinylaniline-activated carbon was then divided in two halves for carrying out positive and negative polymer grafting processes.

For this, the separated half of activated carbon was introduced into a double-necked flask fitted with a reflux system and a magnetic stirrer. For each polymerization, 15 g of the corresponding monomer (sodium 4-vinylbenzenesulfonate as negative, (vinylbenzyl)trimethylammonium chloride as positive), and 18 g of dimethyl sulfoxide (DMSO, obtained from Scharlab, Barcelona, Spain), which acts as solvent, was added to the flask. The mixture was put into an ultrasonic bath for 30-60 minutes. Afterwards, the suspension was kept under stirring at 1000 rpm, and a solution of 95 mg of azobisisobutyronitrile (which acts as polymerization initiator) in 3 mL of DMSO was added to the mixture. Right after adding the initiator, the flask was set to be purged with N_2. After 5 minutes, it was heated up to 70 °C and left overnight. The product was then washed by dispersion in ethanol and centrifuged for 1 hour at 7800 rpm. The supernatant was removed, and the washing process was repeated twice. The resulting product was vacuum-dried at 50 °C overnight and grinded to a fine powder.

Characterization methods

Hydrodynamic particle diameter and electrophoretic mobility determinations were carried out in a ZetaSizer NanoZS instrument from Malvern Instruments (UK). For the observation of the polarization concentration, the experimental method is based on the one described in [30]. A simple microfluidic cell was prepared, in which a carbon disk is introduced. The disks were prepared from a mixture of carbon powder and a 33 g/L solution of poly(vinylidene-fluoride) (PVDF, obtained from Arkema, Colombes, France, as Kynar HSV 900, with an approximate molecular weight of 1 000 000) in 1-methyl 2-pyrrolidone (Sigma Aldrich, Darmstadt, Germany). The weight ratio of the carbon: PVDF solution slurry was 3:10. The tip of a needle (300 µm outer diameter) was diped into the slurry and used to transfer a small amount of the mixture onto a poly(methyl methacrylate) (PMMA) plate, forming a disk-like shape, 500-1000 µm in diameter. Once deposited, the sample was dried overnight at 80 °C. The channel of the observation cell was set up by pressing another PMMA plate onto the carbon-loaded one with an in-between rubber separator, which also works as fluidic channel limiter (see Fig. 4). The resulting chamber is about 500 µm height. The cell is provided with two parallel electrodes made with aluminum conductive tapes, spaced 3.5 cm from each other and connected to a power source.

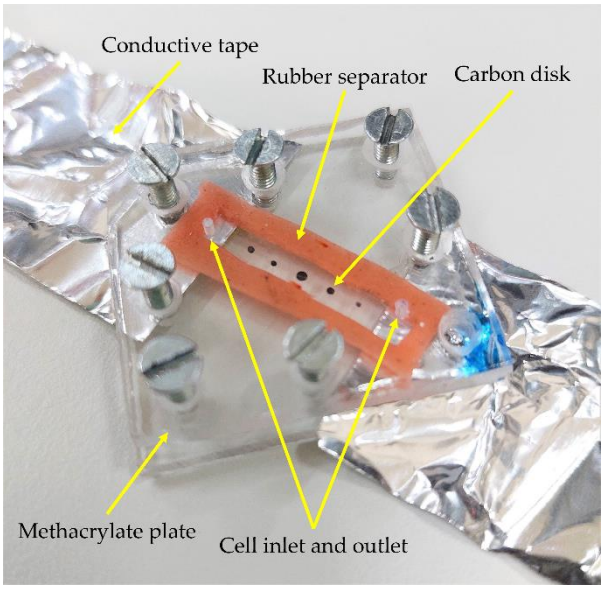

Figure 4. Lab-made microfluidic chamber for the direct observation of concentration profiles around the carbon disks shown. Carbon disks are placed on the lower PMMA plate, and the aluminum conductive tapes were set to be parallel at a distance of 3.5 cm.

The upper PMMA plate was pressed against the lower one, being distanced by an in-between rubber separator. Cell inlet and outlet were carved through the upper plate.

The observation was made by using a Leica DM IL Led inverted fluorescence microscope (Leica Microsystems, Germany) provided with a 4X objective (numerical aperture = 0.1, working distance = 13.9 mm) and a Leica DFC 3000 G CCD camera. A 25 μM rhodamine-B aqueous solution was used as fluorescent agent for the observation. The filtered light used for the sample excitation spans 515-560 nm, and emission takes place at a wavelenght of 580 nm. At t = 0 s, a potential difference of 10 V was applied to the cell electrodes, and this was maintained for a total time of 200 s. Images were captured manually every 20 seconds (and an initial one at t = 2 s) during the process, being the camera set to 70 ms of exposure time.

Image analysis was performed by using a Python script, which transformed the images to greyscale, and then subtracted the i-th image of the bunch from the initial image in order to obtain an absolute difference between the frames. The obtained difference was then normalized between 0 and 255 decimal values. This method was first used on different concentrations of rhodamine-B (25 μM, 10 μM, 5 μM) used as control to obtain a calibration relationship between intensity of fluorescence and concentration. Then, the images were analyzed, and the color-to-concentration map was applied to them.

Since the concentration polarization is so apparent in dielectric dispersion of dispersed systems [38, 39], this technique appears suitable as an additional proof of the existence of EDL polarization. The method, described in, e.g., [40], is based on the determination of the complex impedance of a capacitive cell (a glass cylinder with platinum electrodes in a parallel configuration). By calibration with solutions of known conductivity the complex conductivity can be obtained, and, from this, the real and imaginary components of the electric permittivity as a function of the frequency of the applied ac electric field (typically 1 kHz-2 MHz). It is important to minimize the electrode polarization effect [41], as it can hide the frequency dependence of the permittivity at low-frequencies, making the sought concentration polarization effect practically undetectable. In this work, we use the procedure called *logarithmic derivative* ε_{LD} [42, 43]. It is based on the calculation of the log-derivative of the raw $\varepsilon'(f)$ data, where f is the frequency of the electric field:

$$\varepsilon_{LD}(f) = -\frac{\pi}{2}\frac{\partial \varepsilon'(f)}{\partial \ln(f)} \tag{20}$$

The low-frequency contribution to this quantitty is fitted to a power-law

$$\varepsilon_{LD}(f \to 0) = Af^{-m} \tag{21}$$

and the polarization-corrected dielectric constant can be obtained as follows:

$$\varepsilon_{LD}^{\text{corr}}(f) = \varepsilon_{LD}(f) - Af^{-m} \tag{22}$$

4. Results and Discussion

4.1. Evaluation of the coating

To check whether the coatings were correctly obtained, diameters were measured for bare carbon and polyelectrolyte-coated particles, obtaining (400 ± 120) nm for the bare case, (640 ± 130) nm for the PDADMAC-coated and (462 ± 98) nm for positive grafted carbon. In the case of negative coating, the size with PSS is (460 ± 100) nm and for negative grafting is (474 ± 116) nm. Note the slight increase due to the coatings, even considering the uncertainty in the measurements, due to the polydispersity of the carbon particles themselves. A direct proof of the presence of the polymers was achieved by EDX composition maps of the particle surface. Searching for the presence of chlorine and nitrogen will be an indication of the positive PDADMAC coating, whereas sulphur and sodium can be associated to the negative PSS. Fig. 5 shows some representative pictures: the presence of the mentioned elements is well appreciated on the particles and also forming a sort of halo extending beyond the solid, a typical configuration of adsorbed polymer layers.

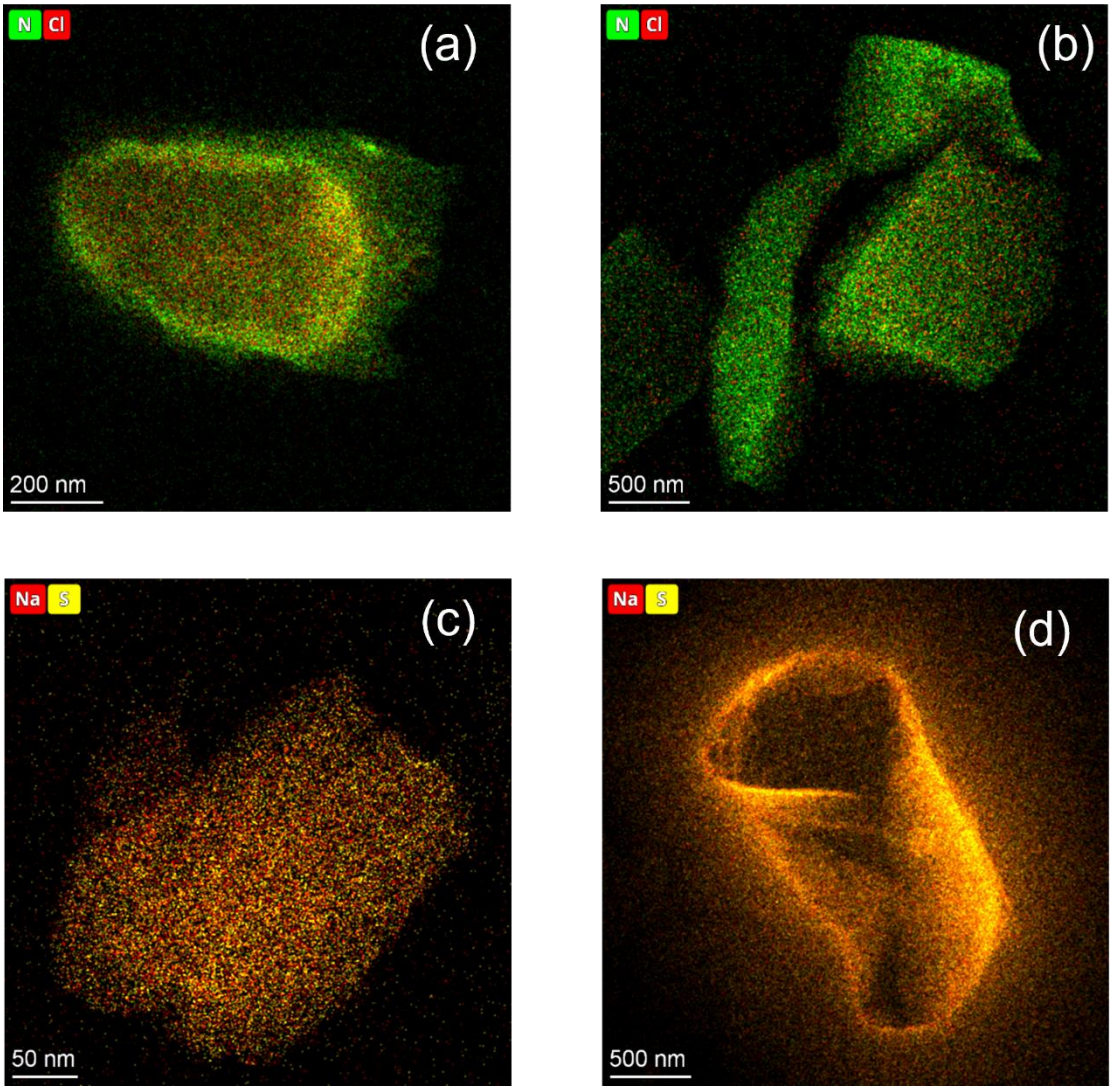

Figure 5. Composition maps of positive (a,b) and negative (c,d) coatings. Left column: adsorbed, and right column: grafted polyelectrolytes.

4.2. Electrophoretic mobility of coated carbon particles

Although a single electrophoretic mobility determination will not be as informative as the set of experiments described below, it can provide a simple view of the electrical nature of the particles.

According to our model predictions, if the carbon particles were perfectly spherical, their electrophoretic velocity would be zero because the net induced charge is zero: the electric field polarizes the electron cloud of the (assumed spherical) conductor, producing oppositely charged EDLs on opposite faces of the particle, and hence no motion at all. The electrophoretic mobility hardly departs from zero at low ionic strengths.

Note, however, that even a small departure from spherical symmetry will distort the situation described, dealing to electrophoretic motion by different EDLs on both sides [44, 45]. Any asymmetry would give rise to unequal electro-osmotic flows and hence a net force towards one of the sides. Since our carbon particles are far from spherical, such asymmetries are very likely, and can vary between different particles. As a result, a wide spectrum of electrophoretic velocities is observed (Fig. 6b).

Another determining factor for the electrophoretic velocity is the difference between the diffusion coefficients of ions in the medium, so it is very interesting to analyze how the velocity spectrum changes with the difference between the diffusion coefficients. If the diffusion coefficients of coions and counterions are different, unequal convective fluxes will be generated, affecting the electrophoretic velocity. Fig. 6a shows that even a change in electrophoretic mobility (u_e) sign can be found, and u_e is positive for NaCl ($D^+ > D^-$), and negative for KCl ($D^+ \cong D^-$) and even more negative for $KBrO_3$ ($D^+ < D^-$). As displayed in Fig. 5b, the mobility spectra are rather wide, enclosing the zero mobility value in the case of KCl.

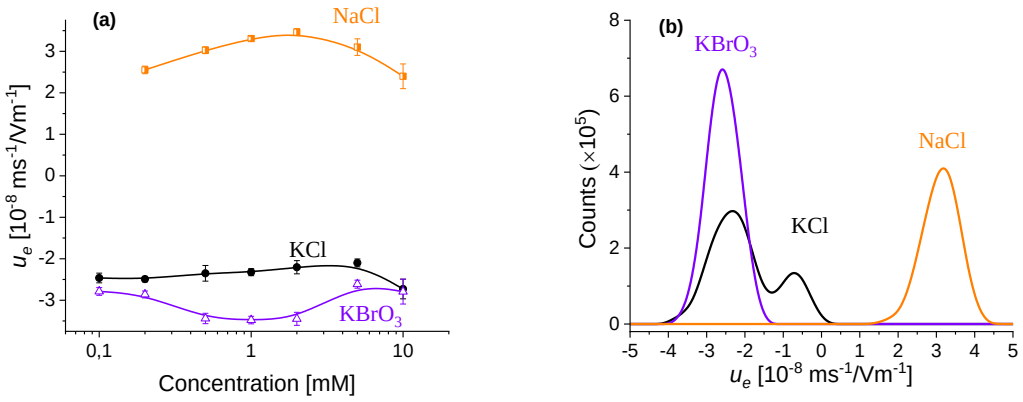

Figure 6. (a) Electrophoretic mobility of bare carbon particles as a function of the concentration of the indicated salts. (b) Mobility spectra (intensity of radiation detected, as a function of mobility) of the same particles for 5 mM concentration.

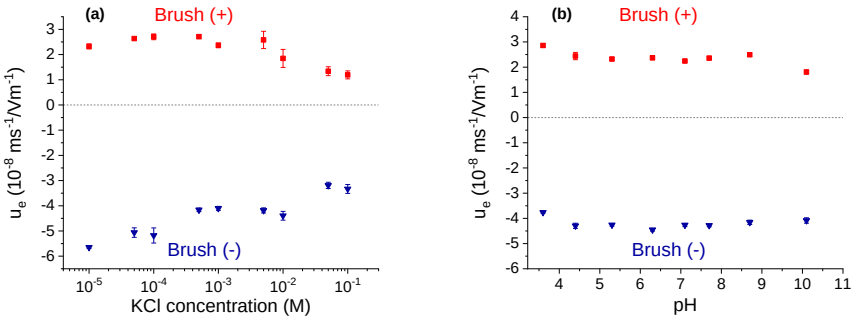

Figure 7. Electrophoretic mobility of carbon particles coated by cationic and anionic polyelectrolyte brushes as a function of KCl concentration (a) and pH (b).

Electrophoretic mobility data are very useful for characterizing the presence of the polyelectrolyte coating and its charge sign. Thus, Fig. 7a shows the mobility as a function of the concentration of KCl, and demonstrates the presence of the layers, more highly charged and less affected by ionic strength in the case of the anionic coating (Brush(-) in the Figure) as compared to cationic one (Brush(+)). Both layers are little modified by pH: it can be admitted that the strong-electrolyte behaviour displayed by both surface treatments makes pH almost irrelevant for electrokinetics of these systems.

4.3. Ionic concentration clouds developed by application of an applied electric field

The applied field on the conducting particle will attract anions from the solution towards the pole on one side, where there is depletion of electrons, and cations at the opposite end. We can speak of a non-uniformly charged EDL, with a charge that will depend (in addition to the radial distance) on the angular position of the point in relation to the axial direction, determined by the external field. If we analyze what happens in a volume at the right pole of the particle (Fig. 8), the induced charge is positive, so that the flow of positive ions in the direction of the field, and therefore entering the volume element, is much smaller than that of negative ions outgoing from it. Away from the DCE, the concentrations of both ionic species are the same, so both fluxes are equal in modulus. As a result, there is a net flux of outgoing ions from that region and thus a salt defect over the right pole. On the left, the surface charge is negative, and the double layer is mostly populated by cations whose flux will be parallel to the field, thus leaving the bulk element. In addition to these electromigratory fluxes, salt gradients produce diffusive fluxes, which

lead this system to reach equilibrium. As a result, over this pole there is also a defect in the neutral salt concentration.

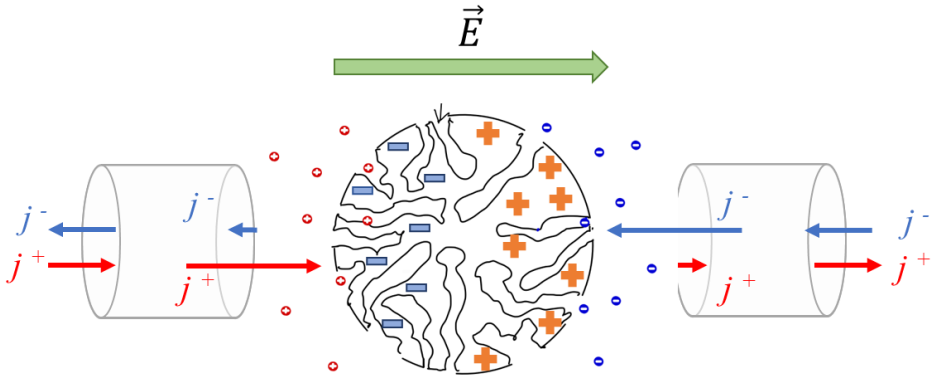

Figure 8. Schematic representation of the electromigratory fluxes at both poles of a porous conductive particle.

In the case of monodispersed spherical particles, the polarization concentration phenomenon produces changes of the ionic concentration that can be calculated on the symmetry axis of the particle as has been done in Ref. [46]. For a 100 nm particle suspended in KCl, with an EDL thickness of equal to $a/10$, and a typical zeta potential of -100 mV, the ratio $\frac{\Delta n(\max)}{n^{\pm}(\infty)}$ is 10^{-6}. This concentration difference has a not measurable impact in direct observation using a fluorescent microscope as such concentration variations are essentially inappreciable. However, in the case of a porous particle, the phenomenon of concentration polarization is magnified and is clearly appreciable as shown in Fig. 9.

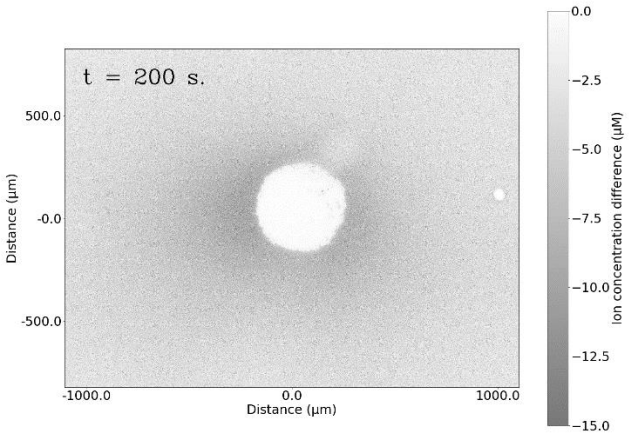

Figure 9. Example of the fluorescence microscope picture obtained when the porous carbon disk is subjected to the action of an electric field of 285 V/m (left to right in the image). The intensity of grey pattern indicates a depletion of the salt concentration on both sides of the particle, after 200 s. Rhodamine B with 25 µM was used in the solution.

By digitizing the images according to the intensity of the fluorescent signal at different times it is possible to determine the temporal evolution of the concentration clouds, as shown in Fig. 10a-c. From the time dependence of the minimum value of concentration (Fig. 10d), it is found that this quantity reaches its final steady value after around 200 s, in agreement with the expected relaxation value for the concentration polarization [39]:

$$\tau_{rel} \cong \frac{a^2}{2D_{eff}} = 128 \text{ s} \tag{23}$$

where $D_{eff} = D^+D^- / (D^+ + D^-) = 7.07 \times 10^{-10}$ m^2/s in the case of rhodamine. Note also in Fig. 10e the very important result that depletion of concentration is found on *both* sides of the particle, although the profiles are not perfectly symmetric, because the particles are not exactly circular, and that the diffusion coefficients of anions and cations are clearly different. The model predictions are presented in Fig. 10f, under the assumption of spherical symmetry. The depletion experimentally found is reproduced by the model, although the lack of symmetry of the particles cannot be captured by the calculations.

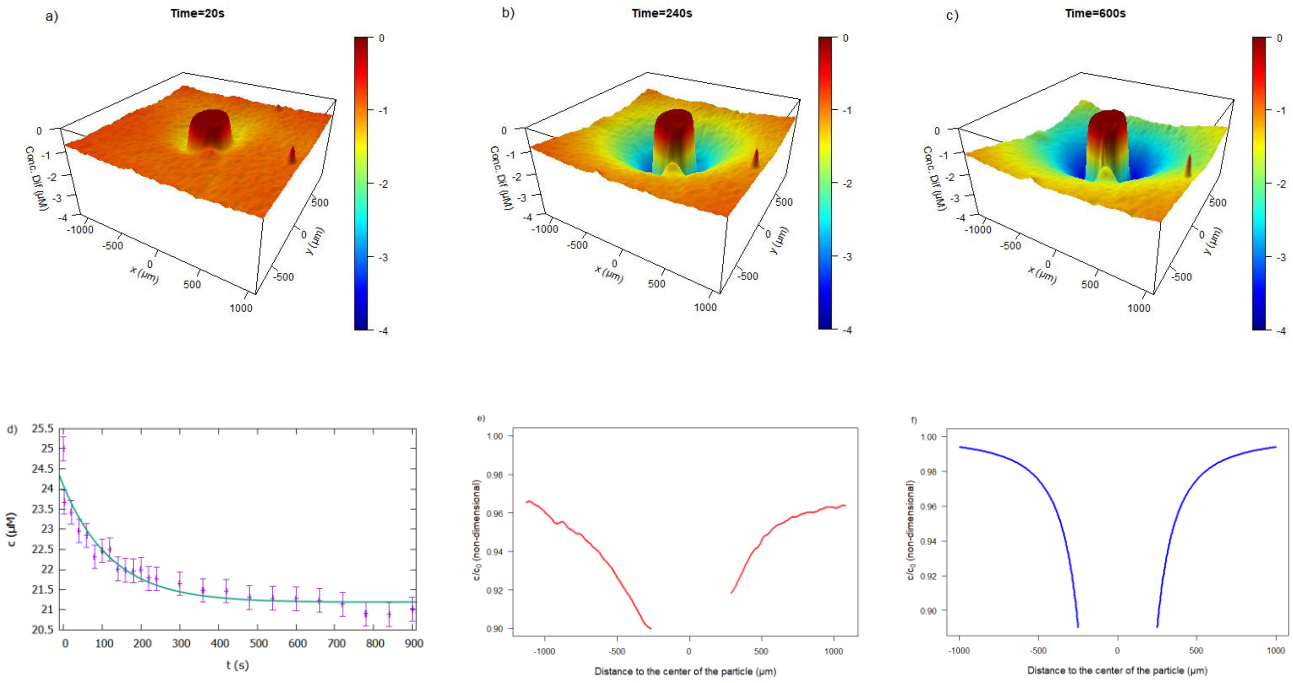

Fig. 10. (a-c): Time evolution of the concentration profiles around a carbon particle 500 μm in diameter as a function of time (up to 600 s as indicated). Panel (d) shows the time evolution of the minimum value of concentration. The steady state is shown in panels (e) and (f) experimentally and theoretically. Rhodamine concentration: 25 μM.

We may now wonder how the patterns shown change when the particles are coated by polyelectrolyte, either adsorbed or grafted. Also, for polyelectrolyte-coated carbon particles here investigated the concentration clouds associated to concentration polarization are clearly visible, as shown in Figs. 11 for the rhodamine dye solution. This fact is demonstrated by the permittivity spectrum reported to the measurements and model of ac electrokinetics of polyelectrolyte brushes carried out in the literature [47, 48].

Wide concentration depletion regions are also established, and we can also observe the very important result that depletion occurs only on one of the particle poles (the right one in the case of positive polymer, and the left in negative coatings), as expected for non-conducting particles [23] with a layer of surface charge. The polymer layer hides to some extent the conducting nature of the core carbon particles. As above mentioned, the observation would be hardly possible for particles with just surface charge, where $\Delta n(\max)/n^{\pm}(\infty)$ would be at most 10^{-5}, not accessible with our

experimental setup. In contrast, the use of porous particles, where the polyelectrolyte coating presumably reaches the walls of the macropores, magnifies the phenomenon and makes it visible with the simple fluorescence microscope.

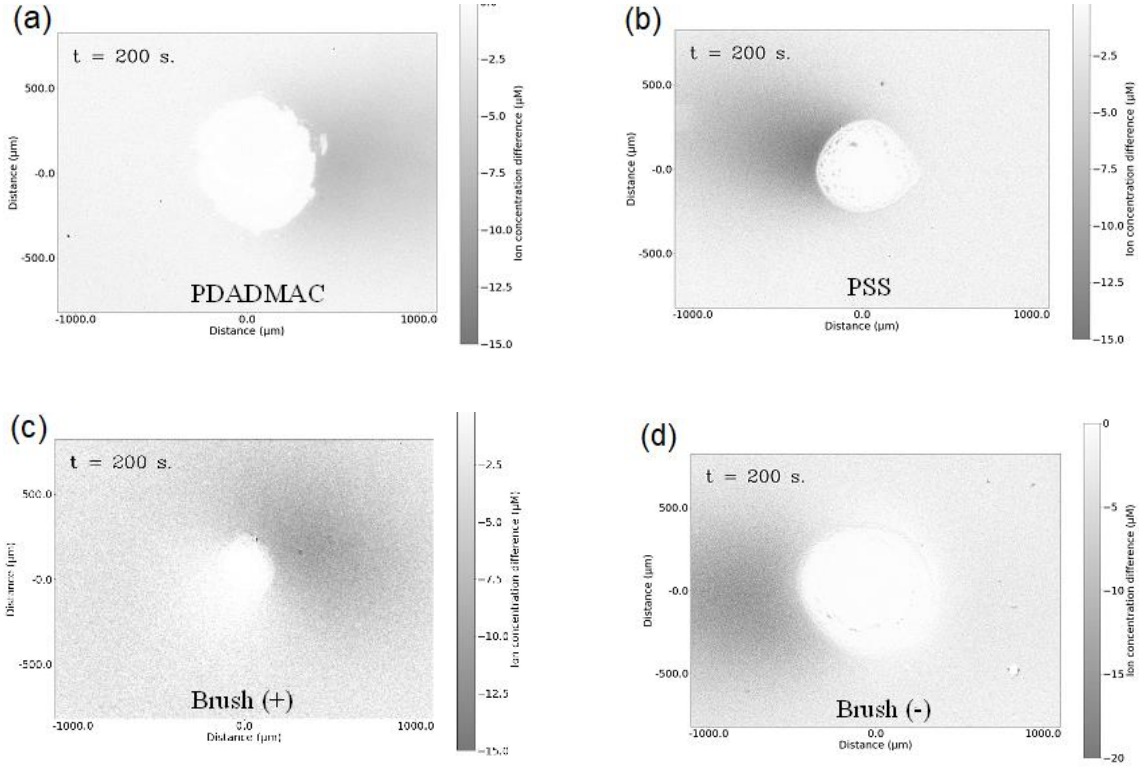

Figure 11. Fluorescence microscope pictures of particles coated by positive (a and c panels) and negative (b and d panels) polyelectrolyte shells. The top row (a and b) corresponds to adsorbed polymers. The bottom panels (c and d) are pictures with grafted polyelectrolytes.

There is an important difference between adsorbed and grafted polymers, beyond the fact that the depletion zone appears more extended in the latter case, and it is that the region of concentration polarization increase is more visible also for grafted layers, and practically inexistent for adsorbed layers. The reason lies on the fact that in the latter case, the polyelectrolyte contributes to the EDL formation just as a thin, soft layer, presumably in the outermost part of the carbon, giving a contribution comparable with that induced by the field and associated to the whole porous structure of the carbon. In contrast, for

grafted layers, the polymer will extend further inside the pores, giving a contribution comparable to that of the pores themselves and screening them. We can conclude that we have achieved a concentration polarization as intense as that of a porous particle but with a pattern (excess on one side and defect on the other) corresponding to that of an insulating particle.

Our model can also contribute to explaining these findings. Using eq. (18), one can calculate the relative concentration changes due to polarization for the different cases analyzed. Thus, Fig. 12 shows the spatial distribution of this quantity for positive and negative polyelectrolytes, either adsorbed or grafted. Note that the regions of concentration increase and depletion due to polarization are clearly distinguishable, whereas only the former is predicted for the case of adsorbed layer.

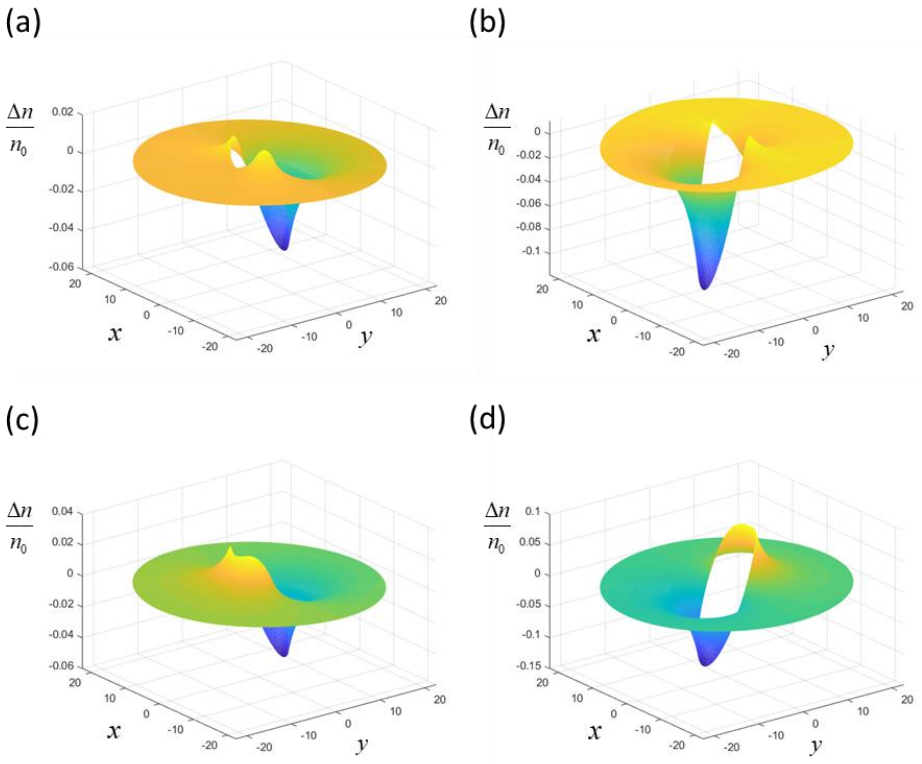

Figure 12. Profiles of relative concentration changes around a carbon disk 500 µm in diameter, calculated using eq. (18) for the following cases: (a): soft, cationic; (b): soft anionic; (c): grafted cationic; (d): grafted anionic. The model assumes that the particle is composed of a 250 nm diameter core, and a 125 nm thick polyelectrolyte layer.

4.4. Dielectric spectroscopy

The dielectric spectroscopy is incredibly sensitive to the polarization concentration phenomena in particles suspended in electrolyte solution. The polarization of the system is strongly affected by the salt concentration gradient formed on both sides of the particle. Thus, an excess on one side and a defect on the other, would imply a deformation of the electric double layer and with this an induced dipole moment opposite to the applied field. But if instead, as predicted by eq. (18), there are no or very small salt differences at the poles of the particle, no alpha relaxation in the electric permittivity should be observed.

Fig. 13 displays the dielectric spectroscopy data of bare and coated carbon particles. The linear dependence of the logarithmic derivative of the dielectric constant found for the lowest frequency range (Fig. 13a) is the manifestation of electrode polarization. After correcting for this effect by subtracting this linear part, the data in Fig. 13b are obtained. This plot visually demonstrates the great difference between the behaviors of the concentration polarization (maximum in the corrected permittivity at low frequency) for bare and coated particles. For the former, the maximum is negligible as compared to the giant relaxation displayed by the grafted polyelectrolyte particles. This is coherent with the direct microscopic observations of polarization concentration in Figs. 9 and 11d: the former, corresponding to the bare carbon, shows just a defect of electrolyte concentration on both sides of the particles, incompatible with a contribution of polarization to permittivity. This explains the quasi-flat frequency dependence of the corrected dielectric constant in Fig. 13a. On the contrary, Fig. 11d demonstrates the existence of the concentration profile by polarization typical in surface-charged particles, i.e., increase of salinity in one pole and decrease in the opposite. In addition, such concentration changes are intense enough to explain the high alpha relaxation in brush-coated particles (Fig. 13b). These results are in agreement with our previous findings on polyelectrolyte coated particles when the polymer layer is hairy and extended far from the particle surface [47, 49].

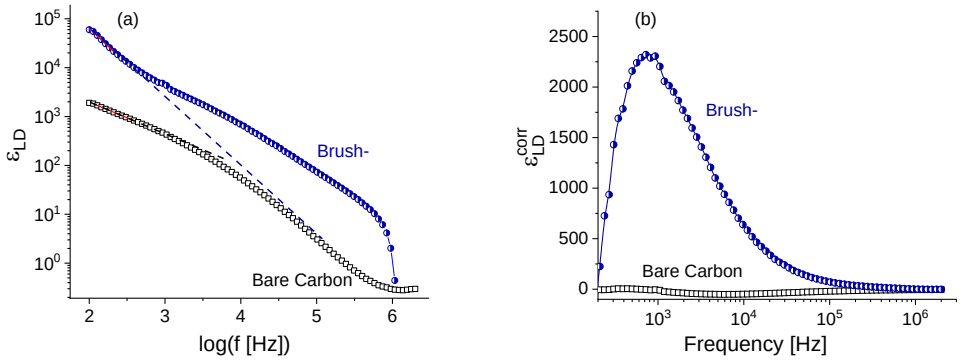

Figure 13. (a) Logarithmic derivative of the real part of the dielectric constant of suspensions of bare and coated (with a negative grafted polymer) carbon particles suspensions. (b) Corrected logarithmic derivative, after subtracting the effect of electrode polarization.

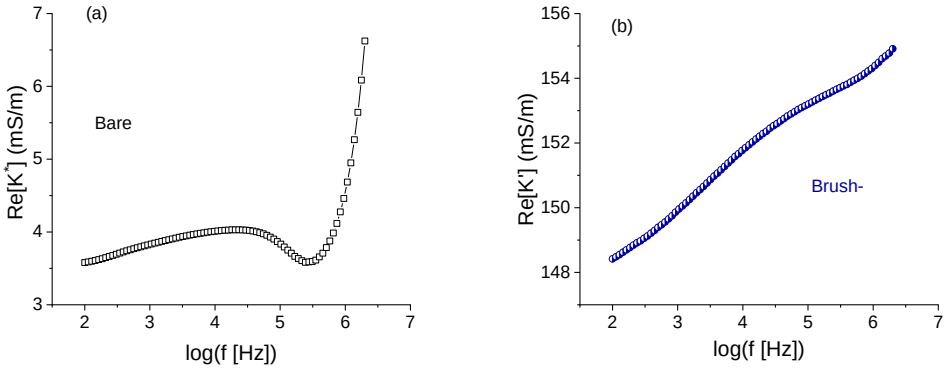

Figure 14. Real part of the complex conductivity of the systems in Fig. 10, both for bare (a) and brush-coated (b) particles.

An intriguing feature of the dielectric constant of the bare particles after correction (Fig. 12b) is the presence of a shallow decrease in ε_{LD} not expected in disperse systems (and in fact not observed for coated particles), where a maximum in this quantity (or, equivalently, in ε'') is normally found, indicating some polarization relaxation mechanism. Such kind of process manifests as an increase in the real part of the conductivity (as in Fig. 14b), that is also inverted for bare particles (Fig. 14a), where a decrease in $\mathrm{Re}[K^*]$ is clearly observed around 10^5 Hz. This behavior might be linked to an inductive (instead of capacitive) process in this kind of systems; classical models on the frequency dispersion of the permittivity do not include such processes. Grosse and

Shilov [50] have proposed that inductive phenomena are possible in porous charged particles (like ion exchange beads), where the different ionic diffusion coefficients of ions inside and outside the particle bring about inertial effects that tend to oppose changes in current direction, that is, inductive behaviour. In our case, the inertia is linked to the difficulties of ions to get in or out of the deepest pores: as the field changes direction, the induced charge on the particles will also undergo the same changes, but ions cannot follow so easily the process as they must abandon the pore and be substituted by the oppositely charged ionic species. Jointly considered, this produces an effect which is qualitatively similar to that described by Grosse and Shilov for ion exchange resin beads.

4. Conclusions

In this work we have presented a model of the buildup of electrolyte concentration gradients (concentration polarization or CP) on both sides (downfield and upfield) of a conducting porous particle in the presence of an external electric field. A model based on the assumption of thin double layers has been elaborated that explains three basic findings: the CP is magnified by the porosity; if carbon particles are bare, only concentration depletions are observed on both sides of the particles; coating them with a layer of polyelectrolyte allows to recover the usual behavior, namely, a pole of the particles is associated to increased electrolyte concentration and the opposite shows depleted electrolyte, magnified in our case by the porosity of the particles. These predictions are observed experimentally using a carbon disk in solutions of a fluorescent dye. Independent tests are based on the evaluation of the dielectric dispersion (i.e., frequency dependence of the electric permittivity of carbon particle suspensions) for both bare and brush-coated particles. It is clearly observed that, while the dependence is close to typical in the case of coated particles, the permittivity of bare conducting particle suspensions shows tendencies that one would associate to inductive, not capacitive processes: the permittivity increases with frequency, something not observed before. This is related to the inertia of the transport processes of ions in and out of the complex pore network of the commercial particles.

5. Acknowledgements

Financial support of this investigation by FEDER/Junta de Andalucía-Consejería de Transformación Económica, Industria, Conocimiento y Universidades, Spain (Grant No. P20_00233) and Consejería de Conocimiento, Investigación y Universidad, Junta de Andalucía, Spain (Grant No. A-FQM492-UGR20) is gratefully acknowledged. Thanks are also due for the grant TED2021-131855BI00/AEI/10.13039/501100011033/Unión Europea Next Generation EU/PRTR.

6. References

[1] V. Presser, C.R. Dennison, J. Campos, K.W. Knehr, E.C. Kumbur, Y. Gogotsi, The Electrochemical Flow Capacitor: A New Concept for Rapid Energy Storage and Recovery, Advanced Energy Materials 2(7) (2012) 895-902.
[2] S.P.S. Badwal, S.S. Giddey, C. Munnings, A.I. Bhatt, A.F. Hollenkamp, Emerging electrochemical energy conversion and storage technologies, Frontiers in Chemistry 2 (2014).
[3] O. Burheim, B.B. Sales, O. Schaetzle, F. Liu, H.V.M. Hamelers, Auto Generative Capacitive Mixing for Power Conversion of Sea and River Water by the Use of Membranes, Journal of Energy Resources Technology-Transactions of the Asme 135(1) (2013).
[4] F. Liu, T.F.W. Donkers, R.M. Wagterveld, O. Schaetzle, M. Saakes, C.J.N. Buisman, H.V.M. Hamelers, Parallel up-scaling of Capacitive Mixing (CapMix) system enhances the specific performance, Electrochimica Acta 187 (2016) 104-112.
[5] O.A. Alvarez-Silva, A.F. Osorio, C. Winter, Practical global salinity gradient energy potential, Renewable & Sustainable Energy Reviews 60 (2016) 1387-1395.
[6] Z. Xia, Z. Wei-Bin, L. Jia-Jun, B. Xu, H. Xiong-Wei, M.T. Myat, X.J. Ma, An electrochemical system for salinity gradient energy harvesting, Energy Conversion and Management 255 (2022).
[7] Y. Oren, Capacitive delonization (CDI) for desalination and water treatment - past, present and future (a review), Desalination 228(1-3) (2008) 10-29.
[8] S.I. Jeon, H.R. Park, J.G. Yeo, S. Yang, C.H. Cho, M.H. Han, D.K. Kim, Desalination via a new membrane capacitive deionization process utilizing flow-electrodes, Energy & Environmental Science 6(5) (2013) 1471-1475.
[9] S. Porada, L. Borchardt, M. Oschatz, M. Bryjak, J.S. Atchison, K.J. Keesman, S. Kaskel, P.M. Biesheuvel, V. Presser, Direct prediction of the desalination performance of porous carbon electrodes for capacitive deionization, Energy & Environmental Science 6(12) (2013) 3700-3712.
[10] B.P. Jia, W. Zhang, Preparation and Application of Electrodes in Capacitive Deionization (CDI): a State-of-Art Review, Nanoscale Research Letters 11 (2016).
[11] A.V. Delgado, M.L. Jimenez, G.R. Iglesias, S. Ahualli, Electrical double layers as ion reservoirs: applications to the deionization of solutions, Current Opinion in Colloid & Interface Science 44 (2019) 72-84.
[12] S. Ahualli, A.V. delgado, Charge and Energy Storage in Electrical Double Layers, Academic Press-Elsevier, London, 2018.
[13] Y. Han, Z.Z. Lai, Z.F. Wang, M.H. Yu, Y.X. Tong, X.H. Lu, Designing Carbon Based Supercapacitors with High Energy Density: A Summary of Recent Progress, Chemistry-a European Journal 24(29) (2018) 7312-+.
[14] C.Y. Zhang, D. He, J.X. Ma, W.W. Tang, T.D. Waite, Faradaic reactions in capacitive deionization (CDI) - problems and possibilities: A review, Water Research 128 (2018) 314-330.
[15] J. Cherusseri, K.S. Kumar, N. Choudhary, N. Nagaiah, Y. Jung, T. Roy, J. Thomas, Novel mesoporous electrode materials for symmetric, asymmetric and hybrid supercapacitors, Nanotechnology 30(20) (2019).

[16] X. Gao, A. Omosebi, Z. Ma, F. Zhu, J. Landon, M. Ghorbanian, N. Kernd, K. Liu, Capacitive deionization using symmetric carbon electrode pairs, Environmental Science-Water Research & Technology 5(4) (2019) 660-671.
[17] P.M. Biesheuvel, A. van der Wal, Membrane capacitive deionization, Journal of Membrane Science 346(2) (2010) 256-262.
[18] J.Y. Lee, S.J. Seo, S.H. Yun, S.H. Moon, Preparation of ion exchanger layered electrodes for advanced membrane capacitive deionization (MCDI), Water Research 45(17) (2011) 5375-5380.
[19] M.M. Fernandez, R.M. Wagterveld, S. Ahualli, F. Liu, A.V. Delgado, H.V.M. Hamelers, Polyelectrolyte-versus membrane-coated electrodes for energy production by capmix salinity exchange methods, Journal of Power Sources 302 (2016) 387-393.
[20] S. Ahualli, G.R. Iglesias, M.M. Fernandez, M.L. Jimenez, A.V. Delgado, Use of Soft Electrodes in Capacitive Deionization of Solutions, Environmental Science & Technology 51(9) (2017) 5326-5333.
[21] S. Ahualli, S. Orozco-Barrera, M.D. Fernandez, A.V. Delgado, G.R. Iglesias, Assembly of Soft Electrodes and Ion Exchange Membranes for Capacitive Deionization, Polymers 11(10) (2019).
[22] P.A. Fritz, R.M. Boom, K. Schroen, Polyelectrolyte-activated carbon composite electrodes for inverted membrane capacitive deionization (iMCDI), Separation and Purification Technology 220 (2019) 145-151.
[23] V.N. Shilov, A.V. Delgado, E. Gonzalez-Caballero, J. Horno, J.J. Lopez-Garcia, C. Grosse, Polarization of the electrical double layer. Time evolution after application of an electric field, Journal of colloid and interface science 232(1) (2000) 141-148.
[24] A. Plecis, R.B. Schoch, P. Renaud, Ionic transport phenomena in nanofluidics: Experimental and theoretical study of the exclusion-enrichment effect on a chip, Nano Letters 5(6) (2005) 1147-1155.
[25] A. Holtzel, U. Tallarek, Ionic conductance of nanopores in microscale analysis systems: Where microfluldics meets nanofluidics, Journal of Separation Science 30(10) (2007) 1398-1419.
[26] P. Montes, J.A.T. Gonzalez, M.E. Araoz, G.L. Iglesias, R.M. Trujillo, R.E. Madrid, A.M. Avila, Renewable carbon-based materials for enhanced ion concentration polarization in sustainable separation devices, Journal of Environmental Chemical Engineering 8(4) (2020).
[27] P.B. Peters, R. van Roij, M.Z. Bazant, P.M. Biesheuvel, Analysis of electrolyte transport through charged nanopores, Physical Review E 93(5) (2016) 14.
[28] Z.B. Gu, B.R. Xu, P. Huo, S.M. Rubinstein, M.Z. Bazant, D.S. Deng, Deionization shock driven by electroconvection in a circular channel, Physical Review Fluids 4(11) (2019).
[29] S. Schlumpberger, R.B. Smith, H.H. Tian, A. Mani, M.Z. Bazant, Deionization shocks in crossflow, Aiche Journal 67(8) (2021).
[30] S. Rubin, M.E. Suss, P.M. Biesheuvel, M. Bercovici, Induced-Charge Capacitive Deionization: The Electrokinetic Response of a Porous Particle to an External Electric Field, Physical Review Letters 117(23) (2016).
[31] H. Lee, D. Kim, J.Y. Kang, K.W. Bong, S.H. Lee, R. Kwak, Nonlinear dynamics of ion concentration polarization in capacitive deionization, Desalination 458 (2019) 14-24.
[32] S.H. Roelofs, A. van den Berg, M. Odijk, Microfluidic desalination techniques and their potential applications, Lab on a Chip 15(17) (2015) 3428-3438.
[33] S. Ahualli, A. Delgado, S.J. Miklavcic, L.R. White, Dynamic electrophoretic mobility of concentrated dispersions of spherical colloidal particles. On the consistent use of the cell model, Langmuir 22(16) (2006) 7041-7051.
[34] C. Grosse, Relaxation Mechanisms of Homogeneous Particles and Cells Suspended in Aqueous Electrolyte Solutions, in: A.V. Delgado (Ed.), Interfacial electrokinetics and electrophoresis., Marcel Dekker, New York, 2002, p. 277.
[35] B.V. Derjaguin, S.S. Dukhin, Nonequilibrium Double Layer and Electrokinetic Phenomena, Surface and Colloid Science, J. Wiley and Sons, N. York, 1974, pp. 273-336.
[36] S.S. Dukhin, V.N. Shilov, Kinetic Aspects of Electrochemistry of Disperse Systems. 2. Induced Dipole-Moment and the Nonequilibrium Double-Layer of a Colloid Particle, Advances in Colloid and Interface Science 13(1-2) (1980) 153-195.

[37] S. Uppapalli, H. Zhao, Polarization of a Diffuse Soft Particle Subjected to an Alternating Current Field, Langmuir 28(30) (2012) 11164-11172.
[38] F. Carrique, F.J. Arroyo, M.L. Jimenez, A.V. Delgado, Dielectric response of concentrated colloidal suspensions, Journal of Chemical Physics 118(4) (2003) 1945-1956.
[39] V. Shilov, A. Delgado, E. Gonzalez-Caballero, J. Horno, J. Lopez-Garcia, C. Grosse, Polarization of the electrical double layer. Time evolution after application of an electric field, Journal of Colloid and Interface Science 232(1) (2000) 141-148.
[40] M.C. Tirado, F.J. Arroyo, A.V. Delgado, C. Grosse, Measurement of the low-frequency dielectric properties of colloidal suspensions: Comparison between different methods, Journal of Colloid and Interface Science 227(1) (2000) 141-146.
[41] H.P. Schwan, Electrode Polarization Impedance and Measurements in Biological Materials, Annals of the New York Academy of Sciences 148(A1) (1968) 191-&.
[42] C. Chassagne, E. Dubois, M.L. Jimenez, J.P.M. van der Ploeg, J. van Turnhout, Compensating for Electrode Polarization in Dielectric Spectroscopy Stuides of Colloidal Suspensions: Theoretical Assessment of Existing Methods, Frontiers in Chemistry 4 (2016).
[43] M.L. Jimenez, F.J. Arroyo, J. van Turnhout, A.V. Delgado, Analysis of the dielectric permittivity of suspensions by means of the logarithmic derivative of its real part, Journal of Colloid and Interface Science 249(2) (2002) 327-335.
[44] N.A. Mishchuk, S. Barany, A.A. Tarovsky, F. Madai, Superfast electrophoresis of electron-type conducting particles, Colloids and Surfaces a-Physicochemical and Engineering Aspects 140(1-3) (1998) 43-51.
[45] M.Z. Bazant, T.M. Squires, Induced-charge electrokinetic phenomena, Current Opinion in Colloid & Interface Science 15(3) (2010) 203-213.
[46] S.E. Pedrosa, C. Grosse, Numerical analysis of the concentration polarization in colloidal suspensions: Comparison with theoretical predictions, Journal of Colloid and Interface Science 219(1) (1999) 37-47.
[47] M.L. Jimenez, A.V. Delgado, S. Ahualli, M. Hoffmann, A. Witteman, M. Ballauff, Giant permittivity and dynamic mobility observed for spherical polyelectrolyte brushes, Soft Matter 7(8) (2011) 3758-3762.
[48] S. Ahualli, M. Ballauff, F.J. Arroyo, A.V. Delgado, M.L. Jimenez, Electrophoresis and Dielectric Dispersion of Spherical Polyelectrolyte Brushes, Langmuir 28(47) (2012) 16372-16381.
[49] S. Ahualli, S. Orozco-Barrera, A.L.M. Castillo, A.V. Delgado, Effect of coating nanostructure on the electrokinetics of polyelectrolyte-coated particles. Grafted vs adsorbed polymer, Journal of Molecular Liquids 375 (2023).
[50] C. Grosse, V.N. Shilov, On the possibility of inductive properties in suspensions of ion exchange resin particles, Journal of Colloid and Interface Science 178(1) (1996) 18-28.